THE UNIVERSITY OF
WARWICK

Original citation:
Cameron, D.T., et al. (2012). Correlated X-ray/ultraviolet/optical variability in the very low mass AGN NGC 4395. Monthly Notices of the Royal Astronomical Society, 422(1), pp. 902-912.
Permanent WRAP url:
http://wrap.warwick.ac.uk/44402

Publisher's statement:
The definitive version is available at www.blackwell-synergy.com
http://dx.doi.org/10.1111/j.1365-2966.2012.20677.x

A note on versions:
The version presented in WRAP is the published version or, version of record, and may be cited as it appears here.

For more information, please contact the WRAP Team at: wrap@warwick.ac.uk

warwick**publications**wrap

highlight your research

http://go.warwick.ac.uk/lib-publications

Correlated X-ray/ultraviolet/optical variability in the very low mass AGN NGC 4395

D. T. Cameron,[1]★ I. McHardy,[1] T. Dwelly,[1] E. Breedt,[2] P. Uttley,[1] P. Lira[3] and P. Arevalo[4]

[1]*School of Physics and Astronomy, University of Southampton, Southampton S017 1BJ*
[2]*Department of Physics, University of Warwick, Coventry CV4 7AL*
[3]*Departmento de Astronomía, Universidad de Chile, Camino del Observatorio 1515, Santiago, Chile*
[4]*Departmento de Ciencias Fisicas, Universidad Andres Bello, Av. Republica 252, Santiago, Chile*

ABSTRACT

We report the results of a 1-yr *Swift* X-ray/ultraviolet (UV)/optical programme monitoring the dwarf Seyfert nucleus in NGC 4395 in 2008–2009. The UV/optical flux from the nucleus was found to vary dramatically over the monitoring period, with a similar pattern of variation in each of the observed UV/optical bands (spanning 1900–5500 Å). In particular, the luminosity of NGC 4395 in the 1900 Å band changed by more than a factor of 8 over the monitoring period. The fractional variability was smaller in the UV/optical bands than that seen in the X-rays, with the X-ray/optical ratio increasing with increasing flux. Pseudo-instantaneous flux measurements in the X-ray and each UV/optical band were well correlated, with cross-correlation coefficients of ≥0.7, significant at 99.9 per cent confidence. Archival *Swift* observations from 2006 sample the intra-day X-ray/optical variability on NGC 4395. These archival data show a very strong correlation between the X-ray and *b* bands, with a cross-correlation coefficient of 0.84 (significant at >99 per cent confidence). The peak in the cross-correlation function is marginally resolved and asymmetric, suggesting that X-rays lead the *b* band, but by ≤1 h. In response to recent (2011 August) very high X-ray flux levels from NGC 4395 we triggered *Swift* target of opportunity observations, which sample the intra-hour X-ray/UV variability. These observations indicate, albeit with large uncertainties, a lag of the 1900 Å band behind the X-ray flux of ∼400 s. The tight correlation between the X-ray and UV/optical lightcurves, together with the constraints we place on the lag time-scale, is consistent with the UV/optical variability of NGC 4395 being primarily due to reprocessing of X-ray photons by the accretion disc.

Key words: accretion, accretion discs – galaxies: individual: NGC 4395 – galaxies: Seyfert – ultraviolet: galaxies – X-rays: galaxies.

1 INTRODUCTION

Almost since their discovery, active galactic nuclei (AGN) have been noted to be variable objects, with flux variations seen in a wide range of time-scales and across the observable electromagnetic spectrum. However, the origin of the ultraviolet (UV) and optical variability in AGN is still a matter of debate. Two mechanisms that have gained support are (i) reprocessing of X-ray emission by the accretion disc (Krolik et al. 1991; Wanders et al. 1997; Collier et al. 1998; Sergeev et al. 2005; Breedt et al. 2009, 2010) and (ii) intrinsic variations of the thermal disc emission (Arévalo et al. 2008; Lira et al. 2011). In scenario (i) the X-ray fluctuations drive and lead the UV/optical

variations; however in (ii), the perturbations are produced in the disc itself, for example, by inwardly propagating accretion rate variations.

In the case of the X-ray reprocessing model, the optical/UV variations are expected to lag behind the X-ray variations, where the length of the lag is determined by the light-travel time from the central compact X-ray emission region to the optical/UV emission region in the disc. Simply from conservation of energy, the absolute luminosity variation in the optical/UV should be smaller than the luminosity variation seen in the (driving) X-ray band. For AGN having black hole masses in the range 10^6–$10^8\,\mathrm{M_\odot}$ (as typically seen in nearby Seyfert galaxies) the lag time-scales are expected to range from seconds to a few days (e.g. Breedt et al. 2009, 2010). The X-ray to UV/optical lag time-scales are expected to increase with observed wavelength (e.g. Cackett, Horne & Winkler 2007),

because the longer wavelength emission is produced at larger radii in the disc.

In the scenario where the UV/optical variations originate in the accretion disc, we expect that these inwardly propagating accretion rate fluctuations will result in the X-ray lagging behind the optical/UV variations. The lag time-scale is then dictated by the viscous propagation time-scale, which is always much longer than the light-travel time, typically months or years for standard accretion discs about black holes having masses 10^6–$10^8 \, M_\odot$ (Czerny 2006).

Of course it is likely that both of these processes are occurring simultaneously within an AGN (e.g. Arévalo et al. 2008, 2009), but we can hope to test which of these processes is causing the *majority* of the UV/optical variation. The nearby Seyfert nucleus in NGC 4395 is perhaps the ideal laboratory in which to test these competing hypotheses, because it is dramatically variable across the X-ray/UV/optical bands and is thought to contain a relatively low mass black hole, meaning that the characteristic time-scales of variations are well matched to the typical durations of intensive observing campaigns (i.e. ≤ 1 yr).

NGC 4395 is a Seyfert 1.8/1.9 galaxy (Filippenko & Sargent 1989) with a black hole mass, estimated from reverberation mapping, of $(3.6 \pm 1.1) \times 10^5 \, M_\odot$ (Peterson et al. 2005). A somewhat smaller black hole mass is suggested by the apparent lack of a significant galactic bulge in NGC 4395, and also from the very short characteristic time-scale measured in the X-ray band (Vaughan et al. 2005). The absolute upper limit on the total mass within the central 3.9 pc, including any stellar contribution, is $6.6 \times 10^6 \, M_\odot$, derived from stellar velocity dispersion measurements (Filippenko & Ho 2003). These black hole mass estimates rank NGC 4395 as one of the very lowest mass AGN known. The distance to the galaxy, derived directly from observations of Cepheid variables, is 4.2 ± 0.3 Mpc (Thim et al. 2004). The proximity of NGC 4395 means that although its luminosity is low in all wavebands, it is bright enough in the X-ray/UV/optical to be observed with short *Swift* snapshots. The very low Galactic extinction, $E(B - V) = 0.017$ mag, in the direction of NGC 4395 (Schlegel, Finkbeiner & Davis 1998) means that it is particularly well placed from the point of view of UV observations, which will not be heavily attenuated.

NGC 4395 has long been noted as a particularly variable AGN, exhibiting large amplitude variations on short time-scales, across many wavebands. For example, a continuous single-orbit (113 ks) *XMM–Newton* observation was analysed by Vaughan et al. (2005). This observation showed the most extreme X-ray variability ever seen in an AGN with a fractional root-mean-squared (RMS) amplitude (F_{var}) of more than 100 per cent in the soft X-ray band (0.2–0.7 keV). Simultaneous optical and near-infrared observations are reported by Minezaki et al. (2006) who estimate the distance to the inner face of the torus in NGC 4395 as ~ 1 light-day providing an upper limit to the size of the accretion disc. The broad line region radius was determined by Peterson et al. (2005, 2006) to be ~ 0.04 pc.

Many of the recent dedicated monitoring campaigns for NGC 4395 have measured lightcurves from either a single or just a few bands spaced closely in wavelength, and have typically not examined the correlated broad-band variability behaviour. For instance, the optical monitor imaging data during the long *XMM–Newton* observation are not well suited to an X-ray/UV/optical variability analysis. Older soft X-ray observations with *ROSAT*, together with a variety of ground-based optical and infrared observations, were presented by Lira et al. (1999). They reported large X-ray flux changes between observations, e.g. by a factor of 2 in

15 d along with 20 per cent changes in optical flux from night to night. However, these authors were unable to comment on the correlation between variations in the optical and X-ray bands due to the non-simultaneity of their data.

The best data set previously available that probes the short-time-scale relationship between the X-ray and UV/optical emission in NGC 4395 has been carried out with coordinated *Chandra*, *Hubble Space Telescope* (*HST*) and ground-based optical observations (e.g. Desroches et al. 2006; O'Neill et al. 2006), in which the UV and X-ray data sets overlap by ~ 10 ks. After cross-correlating the 1350 Å and 0.4–8 keV lightcurves, O'Neill et al. (2006) find an UV lag consistent with zero with an uncertainty of about 25 min. Desroches et al. (2006) present ground-based optical *B*- and *V*-band observations taken in parallel with these *Chandra* observations. The X-ray to optical correlation is rather weak, with a rather flat cross-correlation function (CCF) having a peak correlation coefficient of ~ 0.2. Desroches et al. (2006) estimate that the optical lightcurves lag the X-rays by 44 ± 13 min. The multiwavelength results from the *Chandra*/*HST* *UV*/optical campaign are consistent with a scenario where the optical variations are primarily due to reprocessed X-ray emission. However, these lightcurves span only a few hours, so these observations clearly do not fully sample all of NGC 4395's long-term behaviour. Also, it should be noted that during these observations NGC 4395 was rather faint in the X-ray, with an average flux less than half of that during the previous ~ 100 ks *XMM–Newton* observations (Vaughan et al. 2005). The low flux levels and relatively weak variability in the X-ray, UV and optical lightcurves reduce the ability of the *Chandra*/*HST*/optical data set to constrain the physical parameters of the system.

In order to improve our understanding of the X-ray/UV/optical connection we have carried out a dedicated year-long campaign monitoring NGC 4395 using the NASA Swift observatory (Gehrels et al. 2004). We present the results of these observations which we have analysed together with previous archival *Swift* X-ray and optical monitoring which intensively samples the intra-day X-ray/optical variability. These data are by far the most extensive joint X-ray/UV/optical observations ever made of NGC 4395 and, indeed, of almost any AGN. The multiband *Swift* data allow us to study the correlations and lags between X-ray and UV/optical bands in unprecedented detail and on time-scales from a few hundred seconds up to 1 yr. We note that the *Swift* X-ray lightcurve for NGC 4395 has previously been presented by Kaaret & Feng (2009). In this paper we concentrate on the cross-correlation between the X-ray, UV and optical wavebands; a fuller analysis of the *Swift* X-ray data set will be presented separately (Dwelly et al. in preparation).

The details of the *Swift* observations are presented in Section 2 and the resulting lightcurves are presented in Section 3. In Section 4 we present the cross-correlation results and discuss their implications. In Section 5 we compare the predictions of the standard accretion disc model to the observed behaviour. We summarize our results in Section 6 and present our conclusions.

2 *SWIFT* OBSERVATIONS

2.1 The 2008–2009 long-term data set

We monitored NGC 4395 with *Swift* with ~ 1 ks of exposure time approximately every 2 d during the period 2008 April to 2009 March. There was a break from 2008 August 6 to 2008 October 21 when NGC 4395 was too close to the Sun, thus separating the observations into two well-sampled sections (referred to hereafter as Sections 1 and 2). Useful data were collected by both the X-Ray Telescope

(XRT; Burrows et al. 2005) and the *Ultraviolet/Optical Telescope* (*UVOT*; Roming et al. 2005). Each ∼1 ks observation was subdivided into up to eight separate 'visits', with individual visit lengths ranging from ∼100 to over 1000 s. In total 254 visits were made. Within each visit, the *UVOT* observations were taken through the *uvw2*, *v*, *u* and *b* filters, in that order, with exposure time ratios of approximately 4:1:1:1 for the *uvw2*, *v*, *u* and *b* filters, respectively. The majority of the *UVOT* data were obtained in 'event' mode where the time of arrival and location of each photon are recorded, meaning that we can post-process these data to make images/lightcurves in time bins of arbitrary length.

2.2 The 2006 intensive short-time-scale data set

We have also analysed a set of intensive *Swift* observations of NGC 4395 which were made from 2006 March 6 to 2006 March 10, which we refer to hereafter as the '2006' observations. Throughout this 5 d monitoring period one *Swift* visit of ∼1 ks was made per orbit (i.e. once every ∼96 min), totalling 61 visits. All of the *UVOT* observations of NGC 4395 during this period were made through the *b* filter in 'image' mode, in which a single *UVOT* integration was obtained per visit.

2.3 The 2011 target of opportunity data set

Very recently (2011 August) we have triggered a set of *Swift* target of opportunity (ToO) observations of NGC 4395 in response to a high X-ray flux state. These data consist of six visits spanning ∼13 h, and most importantly, include two relatively long visits of length ∼2500 s. The *UVOT* was operated with the *uvw2* filter and in event mode during these ToO observations.

2.4 Data reduction procedure

The *UVOT* raw data were cleaned, flat-fielded and corrected for mod-8 (fixed pattern noise due to subpixel centralization) noise using the standard *Swift UVOT* pipelines.[1] From an initial examination of the *UVOT* images, we noted that a higher than expected fraction of the visits were affected by poor pointing stability caused by loss of guide star lock, probably due to the scarcity of bright stars at the high Galactic latitude of NGC 4395. Fortunately, the majority of the affected observations were made in event mode allowing the spacecraft attitude information to be corrected on 10–20 s time-scales by tracking the apparent locations of bright stars within the *UVOT* field of view. For each *Swift* observation a series of short snapshot images (10 s for *UVOT* observations in the *u*, *b* and *v* filters, and 20 s for the *uvw2* filter) were created from the raw *UVOT* event lists. Each snapshot was searched for pointlike sources, the apparent positions of which were cross-correlated with a list of bright ($u'_{AB} < 18$) reference stars (obtained from the Sloan Digital Sky Survey (SDSS; Abazajian et al. 2009) catalogue server[2]). A linear offset (in RA and Dec.) to the nominal pointing of the snapshot was then calculated from the crossmatches. A new spacecraft attitude file was then created for each *Swift* observation by applying a filtered and interpolated version of the snapshot offsets to the original spacecraft attitude file. Our astrometric correction method was adapted from routines developed by S. R. Oates for the Swift Gamma Ray Burst catalogue (Roming et al. 2009). This astrometric correction process

was seen to improve the registration of *UVOT* images that were not affected by guide star lock, and so for completeness was applied uniformly to the entire *UVOT* data set. For those visits where the *UVOT* data were obtained in 'image' mode, we calculated only a single pointing correction possible per *UVOT* exposure. We discarded the data from the few visits where the *UVOT* was in image mode which also showed signs of star trailing.

The *Swift*-XRT data reduction procedure will be fully described in Dwelly et al. (in preparation). A brief description of our method can be found in section 2 of Fabian et al. (2012). We note that throughout this work we use X-ray lightcurves that have been corrected for background, vignetting, aperture losses and for the effects of bad pixels.

3 ULTRAVIOLET AND OPTICAL VARIABILITY

Aperture photometry was performed using the *Swift UVOT* tool UVOTSOURCE,[3] with a 3 arcsec radius aperture. The background region was chosen to be representative of the sky near the galaxy. Previous *HST*-Wide Field Planetary Camera 2 (WFPC2) (F815W, ∼ *I* band) observations have revealed that in addition to the central point source, there is a significant galactic contribution within the innermost few arcseconds of NGC 4395 (Filippenko & Ho 2003) which is expected to contaminate our *UVOT* aperture photometry of the nucleus. Note that the point spread function (PSF) of *UVOT* has a full width at half-maximum of ∼2.5 arcsec. We have therefore used archival *HST* observations in the F330W filter (close to *UVOT u* band), the F439W filter (close to *UVOT b* band) and the F555W filter (close to *UVOT v* band), in order to estimate the constant contribution from non-nuclear light to our *UVOT* aperture fluxes. This is possible as the *HST* resolution is ∼50 × better than *UVOT*. We downloaded processed images from the *HST* Legacy Archive website.[4] We used the GALFIT software (Peng et al. 2002, 2010) to fit a galaxy profile model to the central regions (an 18 arcsec by 15 arcsec rectangle) of NGC 4395, adopting the three profile model components of Filippenko & Ho (2003), namely a nuclear point source, a Sersic component representing the nuclear stellar cluster and an exponential disc. Bright irregular features and Galactic stars were masked out during the fitting process. The contribution from the nuclear point-source component was subtracted from the image, which was then convolved with the appropriate *UVOT* PSF model taken from the calibration data base. Finally, the non-nuclear flux within the 3 arcsec radius science aperture was calculated from the convolved image, converting to physical units using the standard *HST* zero-points. We measure the following non-nuclear flux density contributions within the *UVOT* science aperture: 4.9×10^{-16} erg cm^{-2} s^{-1} Å^{-1} in the *u* band, 4.9×10^{-16} erg cm^{-2} s^{-1} Å^{-1} in the *b* band and 5.0×10^{-16} erg cm^{-2} s^{-1} Å^{-1} in the *v* band. No suitable high-resolution UV images were available, so to estimate the non-nuclear flux contamination in the *uvw2* band we normalized the Scd galaxy template of Rowan-Robinson et al. (2008) to the non-nuclear contribution in the *b* band, giving an expected non-nuclear flux of 4.8×10^{-16} erg cm^{-2} s^{-1} Å^{-1} in the *uvw2* band. We subtract these non-nuclear flux estimates from the aperture fluxes calculated within UVOTSOURCE. We expect this procedure to be accurate to around 0.1×10^{-16} erg cm^{-2} s^{-1} Å^{-1} based on the difference between results produced for subtractions using the two archived

---

[1] http://swift.gsfc.nasa.gov/docs/swift/analysis/
[2] http://cas.sdss.org/astrodr7/en/

[3] http://heasarc.nasa.gov/lheasoft/ftools/headas/uvotsource.html
[4] http://hla.stsci.edu/hlaview.html

HST images with the *B* filter. Any systematic offset imprinted on the *UVOT* data by this method will not affect the cross-correlation analysis performed in Section 4. However, any residual systematic flux offsets may affect the results of the accretion disc modelling discussed in Section 5.

In order to verify the stability of the *UVOT* photometry measured by UVOTSOURCE and to refine the default aperture corrections, we have examined the lightcurves of a relatively isolated field star that has a similar apparent magnitude to the nucleus of NGC 4395. We extracted *uvw*2-, *u*-, *b*- and *v*-band lightcurves for this star from the 2008–2009 *UVOT* data set using 3 arcsec apertures and an annular background region, and ignored the few *UVOT* images where the star falls off the edge of the detector. We found that the *UVOT* photometry for this star is stable, with no obvious long-term drifts. We show a summary of the properties of the measured photometry in Table 1. Note that the scatter of the measured fluxes in each of the *uvw*2, *u* and *v* filters is comparable to the nominal uncertainties estimated by the UVOTSOURCE tool. In the *b* filter the error estimates are on average 1.72 times smaller than the true photometric scatter, suggesting that the errors are underestimated for this filter. This additional error is included when the fluxes are corrected for the aperture size. We also measured the lightcurves of the star using the standard 5 arcsec radius aperture, for which the *UVOT* counts to flux density relation has been very accurately calibrated (Poole et al. 2008; Breeveld et al. 2010). Using these values we measure aperture correction values for the 3 arcsec radius aperture. We find that the fraction of light in the 3 arcsec radius aperture is marginally smaller

Table 1. Tests of the accuracy of our *UVOT* photometry as determined from measurements of a star in the field of NGC 4395. N is the number of separate exposures considered for each filter, $\overline{f}$ is the mean flux of the star in each filter in units of 10^{-15} erg s^{-1} cm^{-2} Å^{-1}. $\overline{|f_i - \overline{f}|/\sigma_i}$ is the mean of the ratio of the measured photometric scatter to the nominal uncertainties reported by the UVOTSOURCE tool. The $\overline{cf}$ are the mean aperture correction factors we measure for the star for a 3 arcsec radius aperture.

Filter	$uvw2$	u	b	v
N	197	155	110	153
$\overline{f}$	1.72	6.43	8.72	7.53
$\overline{|f_i - \overline{f}|/\sigma_i}$	0.815	0.94	1.72	1.08
$\overline{cf}$	1.17±0.03	1.10 ± 0.01	1.10 ± 0.01	1.10 ± 0.01

for the *uvw*2 filter than given by the standard *Swift* calibrated value (1.13, 1.10, 1.11, 1.09, in the *uvw*2, *u*, *b* and *v* filters, respectively; Poole et al. 2008). However, we find that the aperture corrections in the *u*, *b* and *v* filters agree closely with those given by the standard calibration. We use the aperture correction values calculated for the test star to correct the 3 arcsec radius aperture photometry for NGC 4395.

The *UVOT* fluxes were corrected for the Galactic reddening of $E(B - V) = 0.017$ mag, by applying the formulae from Roming et al. (2009), to calculate the appropriate correction in each *UVOT* filter. The fully corrected *UVOT* lightcurves are presented in Fig. 1 together with the 2–10 keV XRT lightcurve.
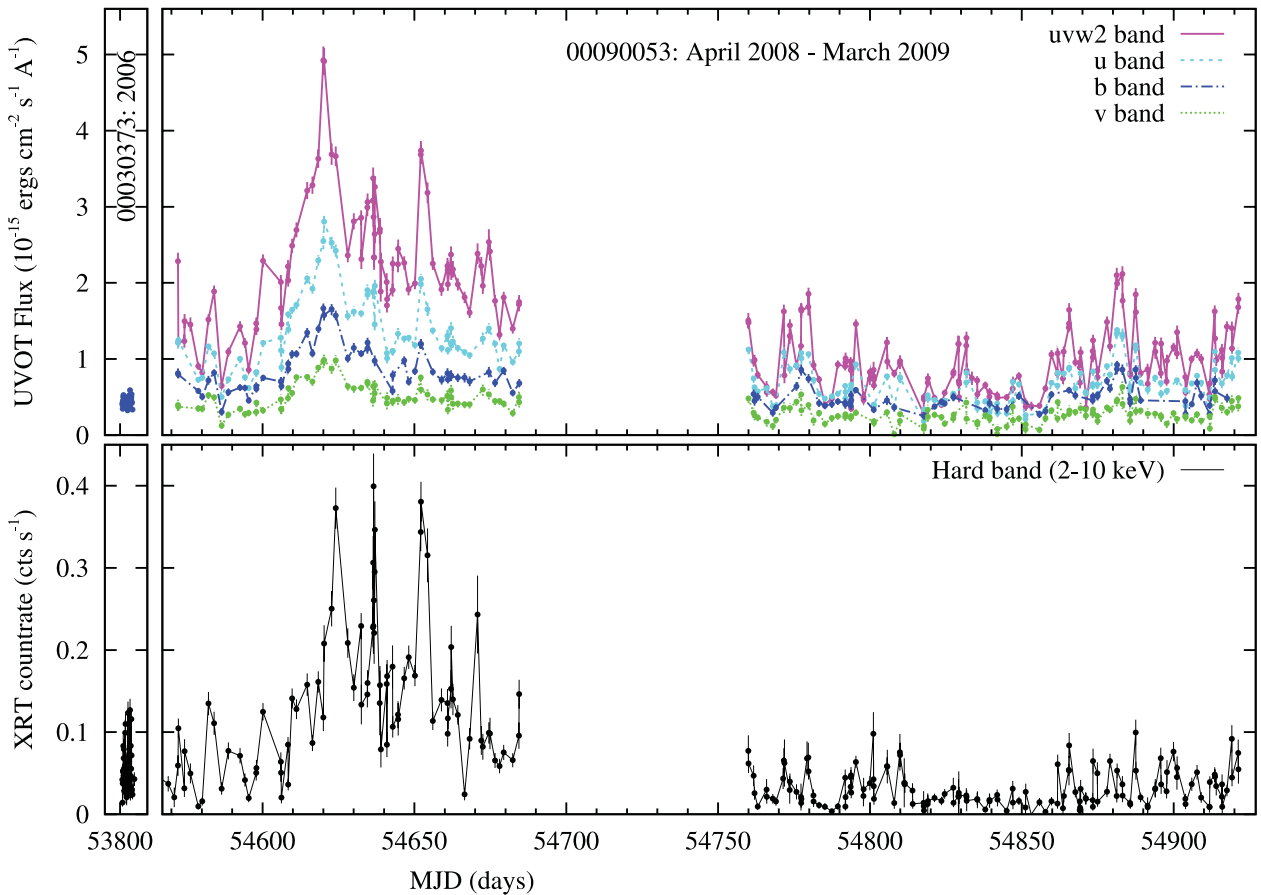
Figure 1. Top panel: lightcurves of the nucleus of NGC 4395 for the *uvw*2, *u*, *b* and *v UVOT* bands. Bottom panel: simultaneous 2–10 keV X-ray lightcurve of NGC 4395, with count rates normalized to account for aperture losses, bad pixels and vignetting. A single data point is shown for each individual *Swift* visit.

Table 2. Central wavelength and fractional RMS variability for the lightcurves measured in each *Swift UVOT* filter. λ is the central wavelength of the filter. F_{var1} and F_{var2} are the fractional RMS variability for the first and second sections of the 2008–2009 observations, respectively.

| Filter	λ (Å)	F_{var1}	F_{var2}
*uvw*2	1928	0.367 ± 0.017	0.427 ± 0.032
u	3465	0.355 ± 0.017	0.395 ± 0.032
b	4392	0.347 ± 0.022	0.325 ± 0.035
v	5468	0.347 ± 0.042	0.420 ± 0.089

3.1 Long-term variability

During the 2008–2009 observation period, NGC 4395 showed significant variability across all *UVOT* filters, Fig. 1. We calculated the fractional RMS amplitude (F_{var}) separately for each of the two contiguous sections of the lightcurve, and the results are shown in Table 2. The fractional variabilities for each filter and during both sections are consistent. This is expected for observations of similar lengths (Uttley & McHardy 2001). The peak-to-trough variation during section 1 is larger than that in section 2, with the *uvw*2-band peak flux approximately eight times greater than the minimum flux. During section 1, NGC 4395 reached an UV/optical flux approximately twice that of the typical peak fluxes of previous observations (Lira et al. 1999; O'Neill et al. 2006).

3.2 Short-term variability

We reduced the *Swift UVOT* and XRT data obtained during the intensive monitoring observations in 2006 in exactly the same way as described in Section 3.1. The *b* filter and X-ray lightcurves are shown in Fig. 2. The fractional RMS of the *b*-band lightcurve during this period was only 0.122 ± 0.006, which is less than a third of variability observed during the 2008–2009 observations. This reduction is to be expected due to the red noise nature of AGN lightcurves, in which the largest amplitude of variability is found on the longest time-scales. However, significant variability with an amplitude greater than the measurement error is still seen on a time-scale of one or two orbits within the 2006 data set.
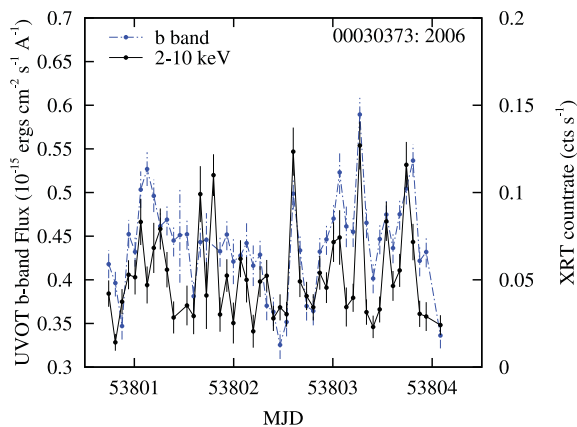
Figure 2. The *UVOT b* band, and XRT 2–10 keV lightcurves of NGC 4395 from the 2006 intensive monitoring data. One point is shown per *Swift* visit. Visits are typically separated by approximately 96 min. Note that the *b*-band lightcurve is shown with a non-zero intercept (left-hand scale) to emphasize the variations.

3.3 Very short term variability

For those *UVOT* data that were collected in event mode we are able to generate lightcurves with arbitrary time binning. In principle, this permits us to investigate lags on time-scales shorter than the length of a whole *Swift* visit (typically ~100–1000 s), but due to the typically rather low XRT count rate measured for NGC 4395 one cannot usually subdivide the *Swift* visits whilst retaining a high-signal-to-noise lightcurve. However, during the brightest outbursts from NGC 4395 we measure count rates >0.5 counts s^{-1} in the XRT, and so lightcurves with binning of 200 s are feasible. We first examined the short-time-scale X-ray/UV/optical variability in the 2008–2009 data set during the epochs when NGC 4395 was at its brightest. Unfortunately, because the exposure time in each *Swift* visit was spread between four *UVOT* filters the range of lag time-scales covered was small. It was not possible to derive a useful measure of the lag between any single *UVOT* waveband and the X-ray band. There was a very small bump in the cross-correlation hinting that the lag could be ~200 s.

To improve on these tentative findings we instigated a new long-term *Swift* monitoring programme (starting 2011 April and scheduled to finish in 2012 March) to search for (and respond to) occasions when NGC 4395 was sufficiently bright that X-ray/UV variability on 100–200 s time-scales could be detected with high confidence. Our monitoring revealed that NGC 4395 had again reached a high X-ray flux level in 2011 mid-August and so we triggered a pre-approved ToO to obtain long (>2 ks) continuous observations using just the *uvw*2 filter. Unfortunately NGC 4395 was just about to enter the *Swift* Sun avoidance region, and so we only obtained ~7 ks of data. The resulting lightcurves are shown in Fig. 3.

3.4 X-ray flux–UV/optical flux relation

In Fig. 4 we show the relationships between the quasi-simultaneous X-ray count rate and *UVOT* fluxes for the nucleus of NGC 4395. We can see that there is a tight correlation between the X-ray and UV/optical bands with very few outlying points.

In Fig. 4 we also show the X-ray versus *b*-band relationship measured during the 2006 intensive monitoring campaign. The 2006 data clearly follow a different track to the 2008–2009 measurements, with a much lower *b*-band flux for a given X-ray count rate, with an apparently flatter slope. As a first step in trying to understand the difference we parametrize the relationship by $F_b = A + B \, F_X^C$.
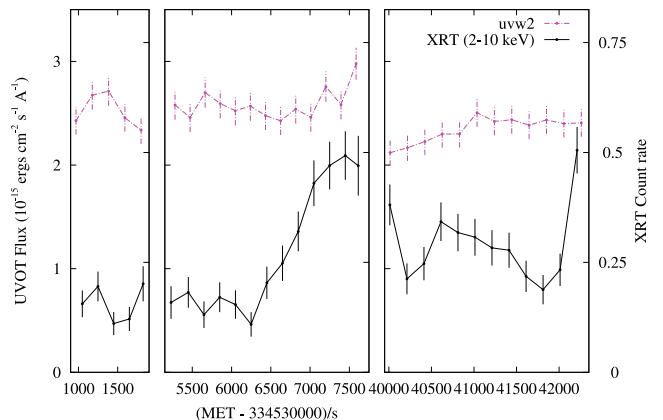
Figure 3. The *UVOT uvw*2 band, and XRT 0.5–10 keV lightcurves of NGC 4395 from the 2011 August ToO observations. One point is shown per 200 s.
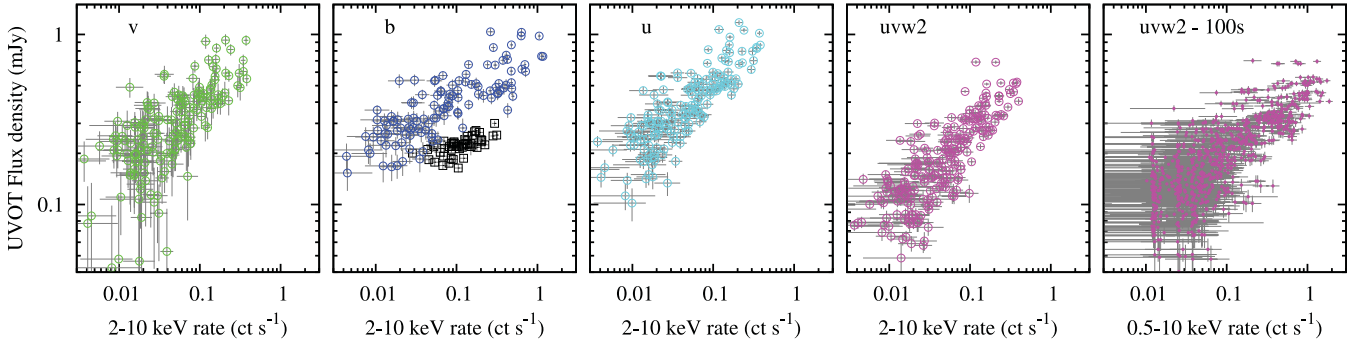
Figure 4. Plots of the 2–10 keV X-ray count rate versus the instantaneous UV/optical flux density. We show data from the long time-scale monitoring campaign (2008–2009), with the *UVOT* filter indicated in the top-left corner of each panel. In the first four panels from the left we show one data point per *Swift* visit. Note that in the *b*-band panel we also show data from the short-time-scale monitoring observations in 2006 (black squares). In the rightmost panel we show the X-ray and *uvw2* data sampled on 100 s time-scales. In this panel we plot the full band 0.5–10 keV count rate to maximize the number of photons per 100 s bin The grey lines represent the 1σ uncertainties.

Here A could be any constant component in the *b*-band flux. The fitted value of A is similar for both data sets ($\sim 0.15 \pm 0.06$ mJy) and the exponents (C) are also similar (~ 0.6), but the slopes (B) differ [0.4 ± 0.3 mJy (count s^{-1})$^{-1}$ for the 2006 data and 1.2 ± 0.15 mJy (count s^{-1})$^{-1}$ for the 2008–2009 data]. We note that due to the large spread in the data the fits are statistically poor and so we do not place too much significance on these values.

Although the exact shape of the *b*-band/X-ray relationship is not well defined, the lower *b*-band flux for a given X-ray count rate in the 2006 observations is clear. This could be due to there being a reduced long-term average accretion rate during these observations relative to that in the 2008–2009 observations. This would reduce the temperature of the accretion disc and thus the flux in the *b*-band from the disc, even if the X-ray count rate is similar.

4 CROSS-CORRELATIONS

We have examined in detail the cross-correlation between the X-ray and UV/optical lightcurves. We calculate the CCF using the hard X-ray (2–10 keV) count rate as a proxy for the intrinsic X-ray luminosity. The hard band count rate is expected to be a better representation of the intrinsic luminosity because it is less sensitive to obscuration (Dwelly et al., in preparation). We used the discrete cross-correlation method (DCF; Edelson & Krolik 1988) adopting 2 d binning for the 2008–2009 long-term monitoring data and 96 min binning (similar to the *Swift* orbital period) for the 2006 intensive monitoring data. We have examined the range $-40 <$ lag $< +40$ d for the long-term monitoring data set and $-1 <$ lag $< +1$ d for the intensive monitoring. We have also examined shorter time-scales by subdividing event mode data, see Section 4.3 below.

4.1 Long time-scales

4.1.1 X-ray–UV/optical cross-correlation functions

In Fig. 5 we show the CCFs calculated by correlating the 2–10 keV X-ray 2008–2009 lightcurve with each of the *UVOT uvw2*-, *u*-, *b*- and *v*-band lightcurves. We have first calculated a separate CCF for each of the two contiguous sections of the 2008–2009 *Swift* data set. The combined CCF for the entire 2008–2009 data set was determined by taking the average value of the CCFs for each of the two sections, weighted by the relative time spanned by each section.

We see that each of the CCFs (in each *UVOT* filter and for each subsection of the data) have a similar structure, and all show a very

strong sharp peak at zero lag. The temporal resolution of our 2008–2009 *Swift* lightcurves is of the order of 2 d, so the peaks in the CCFs are constrained to be less than 2 d, i.e. consistent with zero lag. These small lags are consistent with a reprocessing scenario as long as the light-travel time from the central X-ray source to the UV/optical emission region is less than 1 d.

For a standard thin accretion disc with a constant accretion rate, Shakura & Sunyaev (1973) predict the disc temperature, in kelvin, as a simple function of radius,

$$T(R) = 1.2 \times 10^8 \left[\frac{\dot{m}}{\dot{m}_{\rm Edd}} \frac{M_\odot}{M_{\rm BH}} \left(\frac{R_{\rm g}}{R} \right)^3 \left(1 - \sqrt{\frac{6R_{\rm g}}{R}} \right) \right]^{1/4}, \quad (1)$$

where $M_{\rm BH}$ is the black hole mass, $M_\odot$ is the mass of the sun, $\dot{m}$ is the accretion rate and $\dot{m}_{\rm Edd}$ is the Eddington accretion rate.

So, for a black hole with mass 10^5 M$_\odot$ having an accretion rate of 1 per cent Eddington, we expect from the standard thin disc model that the part of the disc which is emitting at $\lambda_{\rm peak}$ will lie at a radius,

$$R(\lambda_{\rm peak}) = 625 R_{\rm g} \left(\frac{M_{\rm BH}}{10^5 \, M_\odot} \right)^{-\frac{1}{4}} \left(\frac{\dot{m}_{\rm Edd}}{0.01} \right)^{\frac{1}{4}} \left(\frac{\lambda_{\rm peak}}{3500 \, \text{Å}} \right)^{3/4} \quad (2)$$

from the black hole. Note that we have neglected the $\sqrt{\frac{6R_{\rm g}}{R}}$ term as it is <1 at the radii that are responsible for the bulk of the UV/optical emission. Therefore, for NGC 4395 with an assumed black hole mass of 10^5 M$_\odot$, we expect that the part of the disc that is emitting at a peak wavelength of 3500 Å (i.e. approximately the *UVOT u* band) will lie at a radius of $625 R_{\rm g}$, which is around 300 light-seconds. Therefore, the constraints on the lag time-scale derived from the 2008–2009 data set (≤ 2.0 d) are fully consistent with the expected reprocessing time-scale.

A close examination of the CCF peaks shown in Fig. 5 reveals that there is a slightly asymmetric shape to the CCF peaks derived from the first section of the 2008–2009 data set. This asymmetry is apparent in the CCFs for all four *UVOT* bands, appearing in the sense that the CCF peak declines more slowly towards UV/optical leads than towards X-ray leads. This asymmetry is likely caused by the section of the lightcurves near MJD ~ 54600 (see Fig. 1) where the UV/optical lightcurves start to rise earlier (at MJD ~ 54595) than the X-ray lightcurve rise (at MJD ~ 54608). We do not see the asymmetry in the CCF peak in the second section of the 2008–2009 data set.

We see from Table 3 that there is a trend of decreasing peak CCF strength with increasing central wavelength of the *UVOT* filter. This trend is consistent with the reprocessing model since the
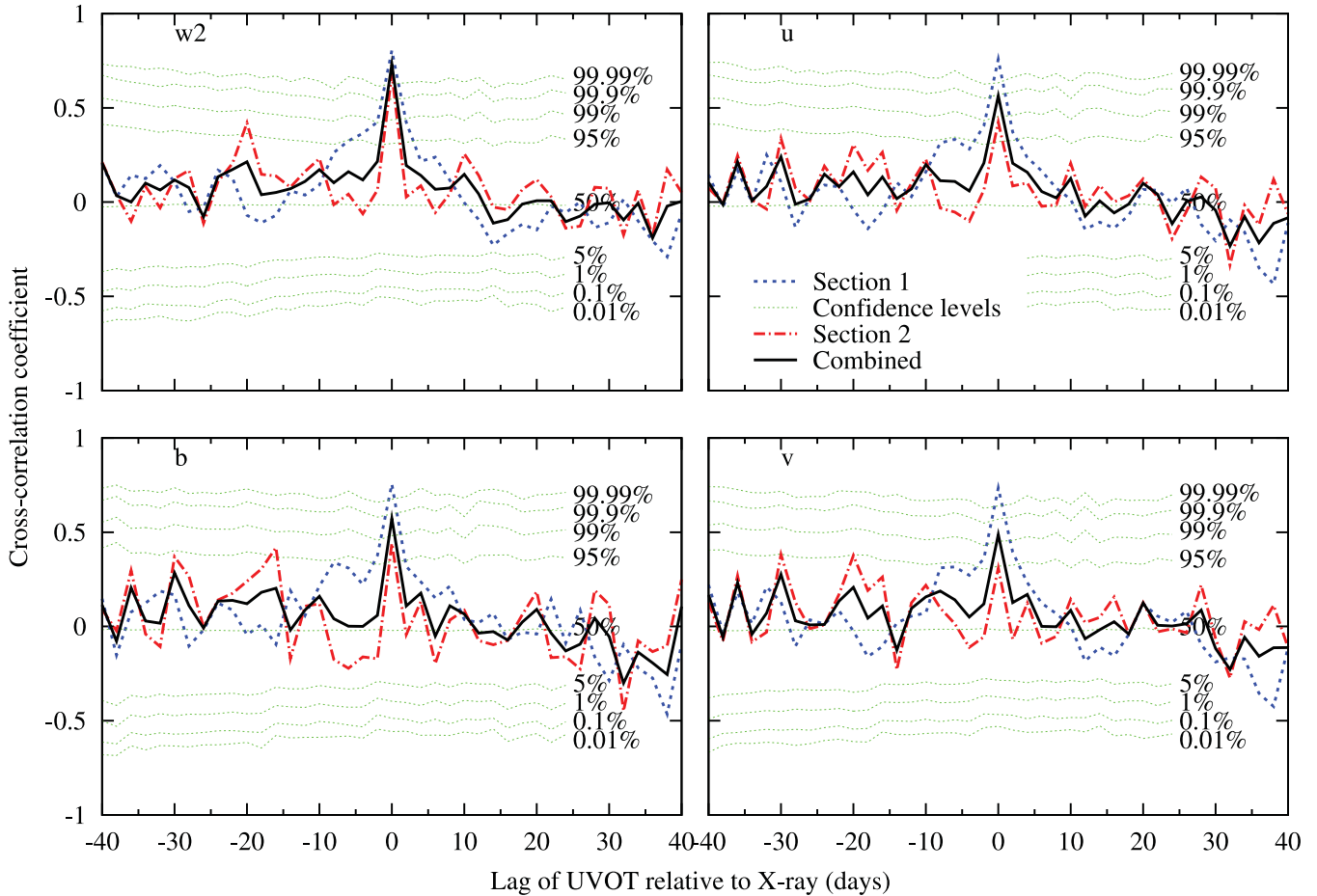
Figure 5. The long-term CCFs between the 2–10 keV X-ray lightcurve and the lightcurves in the *uvw2, u, b* and *v UVOT* bands. The *UVOT* band is indicated in the top-left of each panel. Separate curves are plotted for the first (blue dashed line) and second (red dot–dashed line) sections of the 2008–2008 data set, as well as for the combined CCF (black solid line). The dotted (green) contours are derived from Monte Carlo simulations and indicate the cross-correlation values that a CCF feature must have to be considered significant at the given confidence level. The contours shown are appropriate for a single trial (i.e. at a given lag) and are for the first section of the 2008–2009 observations.

Table 3. The strength of the X-ray to UV/optical cross-correlation at zero lag, as derived from the 2008–2009 data set. DCF is the discrete cross-correlation coefficient at zero lag and Sig is its local significance. Results are shown separately for each section of the long-term *Swift* monitoring (section 1 is 2008 April–2008 August and section 2 is 2008 October–2009 March). The significances are calculated from the percentage of 100 000 Monte Carlo simulated lightcurves having smaller cross-correlation values at zero lag than the observed DCF values.

	Section 1		Section 2	
UVOT filter	DCF	Sig	DCF	Sig
uvw2	0.80	99.9 per cent	0.68	99.9 per cent
u	0.76	99.9 per cent	0.42	99.9 per cent
b	0.76	99.9 per cent	0.44	99.8 per cent
v	0.73	99.9 per cent	0.31	98.4 per cent

longer wavelength light is believed to come from the cooler regions of the disc further away from the central X-ray emission region. Increasing the distance of the reprocessor from the black hole results in the reprocessing region subtending a smaller solid angle as seen from the X-ray source, reducing the fraction of the X-ray emission that can be reprocessed. For reprocessing of X-ray photons from a

point source by a disc, lags are observed that are dependent on the increased travel time to the reprocessing material and also on the distance from the reprocessing material to the observer. For example, the predicted lag for a disc inclined at an angle θ where $\phi = 0$ is the most direct line to the observer is given by

$$\Delta t = \frac{\sqrt{H_x^2 + R^2} + H_x \cos\theta - R \sin\theta \cos\phi}{c}, \qquad (3)$$

where Δt is the increased travel time for the reprocessed emission compared with the direct X-ray emission, H_x is the height above the disc, R is the radius of the reprocessor, θ is the inclination angle, ϕ is the azimuthal angle and c is the speed of light. The longer wavelength emission arises from larger radii in the disc increasing the spread of light-travel times for a disc with non-zero inclination. The optical emission region also spans a larger range of radii than the UV emission region. The combination of these factors results in the transfer function relevant to the reprocessing of a δ-function X-ray impulse into UV/optical emission being broader for longer wavelengths.

We have assessed the significances of the observed CCF peaks using Monte Carlo simulations (see e.g. Breedt et al. 2010). We generate simulated X-ray lightcurves according to the method of Timmer & Koenig (1995), adopting the X-ray power spectral density parameters for NGC 4395 determined by Vaughan et al.

(2005), scaled to the mean and RMS of the observed 2–10 keV *Swift*-XRT lightcurve, and taking account of the actual sampling pattern in the *Swift* data set. The simulated X-ray lightcurve was then cross-correlated with each of the observed *UVOT* lightcurves to produce a simulated CCF, using the same CCF time axis binning as adopted for the actual science data. This process was repeated for a large number ($>10^5$) of simulated X-ray light curves. The resultant ensemble of simulated CCFs, which by construction should contain no real correlated signal, allows us to calculate the probability of finding a particular correlation coefficient at a given lag time by chance. A separate set of simulations is carried out for each of the subsections of the data (i.e. the two sections of the 2008–2009 monitoring and the 2006 data set are all treated separately). If we decide in advance which lag we are searching for, e.g. zero lag, then we can estimate the significance of the zero-lag peaks by determining the fraction of simulated lightcurves that have a CCF value (at zero lag) that exceeds the measured peak CCF value. The CCF strength and the statistical significances of the observed zero-lag peaks are shown in Table 3. We find that for the first section of the 2008–2009 data set, and for each *UVOT* filter, the detected CCF peaks at zero lag each have a significance of at least 99.9 per cent. During the second section of the 2008–2009 data set the peak cross-correlation strength is somewhat reduced for all four *UVOT* filters (see Table 3). However, the peak at zero lag still has a significance of at least 99 per cent for all but the *v* band, which itself is significant at >98 per cent confidence.

4.1.2 *UVOT–UVOT cross-correlation functions*

We have also used the 2008–2009 lightcurves to calculate the cross-correlations *between* the *UVOT* bands. An example UV/optical CCF (between the *v* and *uvw2* bands) is shown in Fig. 6. We find that all *UVOT* bands show very strong correlations with each other and the CCFs calculated for any combination of *UVOT* bands show a peak with a lag of zero days, consistent with the hypothesis that the majority of the optical emission is produced by reprocessing of the X-ray emission. If the disc fluctuations were the dominant cause of the UV/optical variability the longer wavelength emission would be expected to lead the shorter wavelength emission with lags dependent on the viscous time-scales for an accretion disc. These are substantially longer than the observed lags. We see in Fig. 6 that
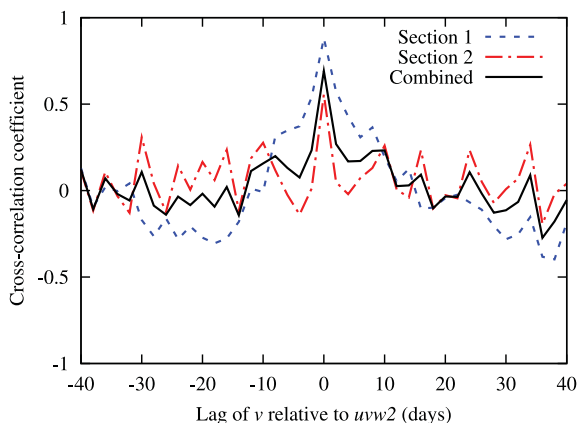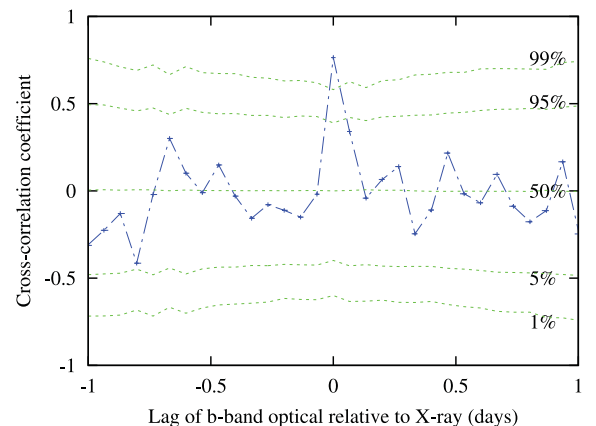
the peak of the CCF is stronger and broader when calculated for just the first section of the 2008–2009 data set (this is also true for most combinations of *UVOT* bands). We do not see any indication that there is a strong asymmetry of the main CCF peak, but weaker features do appear at lags of ±18–20 d in the CCF calculated for the second section of the 2008–2009 data set.

### 4.2 Short-time-scale cross-correlation functions

We have examined the intra-day relationship between the optical and X-ray emission from NGC 4395 using the 2006 *Swift* intensive monitoring data set. We calculated the CCF between the 2–10 keV X-ray and the *UVOT b*-band lightcurves using the DCF method, with a bin size of 96 min (equal to the orbital period of the *Swift* satellite). We plot the result in Fig. 7 and see that the CCF is very strongly peaked at zero lag, with a peak cross-correlation coefficient of 0.84, dropping rapidly either side of zero lag. This sharp drop in the CCF indicates that the peak. Therefore, we infer that peak cross-correlation between the *b* band and X-ray lightcurves must occur at a lag shorter than 48 min (i.e. half the bin time). We note that for an $\sim10^5$ M$_\odot$ black hole, 48 light minutes corresponds to $6000R_g$. The statistical significance of the zero-lag peak in the CCF is >99 per cent, determined using a set of Monte Carlo simulations (similar to those described in Section 4.1.1).

A close examination of Fig. 7 reveals that the peak is slightly asymmetric towards a positive lag, hinting that the optical lightcurve lags the X-ray lightcurve, consistent with the results of Desroches et al. (2006). The shape of the CCF peak derived from the 2006 *Swift* data set is sharper and reaches a much higher correlation coefficient than the CCF presented in fig. 13 of Desroches et al. (2006, who used X-ray and UV data from *Chandra* and *HST,* respectively). The 2006 *Swift* CCF drops rapidly to near zero for lags with $|t_{\text{lag}}| > 2$ *Swift* orbits, and is well determined out to lags of ±1 d. Therefore, the X-ray/optical CCF derived from the 2006 *Swift* data set constrains very strongly the location of the reprocessing region relative to the central X-ray source.

The disc reprocessing transfer function relating the X-ray input to the UV/optical emission can be parametrized fairly accurately by a very sharp rise followed by an exponential decay (Breedt et al. 2009). To estimate the width of this function we convolved the hard

Figure 6. The CCF between the lightcurves in the *uvw*2 and *v* filters, derived from the 2008–2009 *UVOT* monitoring of NGC 4395. Note the very strong cross-correlation at zero lag. Positive lags would indicate that *v* lags behind *uvw*2. Sections 1 and 2 refer to the first and second contiguous sections of the 2008–2009 data set, respectively.

Figure 7. The short-time-scale (<1 d) CCF between the X-ray and *b* bands calculated for the 2006 intensive monitoring data set (blue dot–dashed curve). Significance levels derived from Monte Carlo simulations are shown with (green) dotted lines. The CCF clearly shows a significant and very narrow peak at zero lag. The points are binned on 96 min time-scales, which corresponds to approximately one *Swift* orbit.
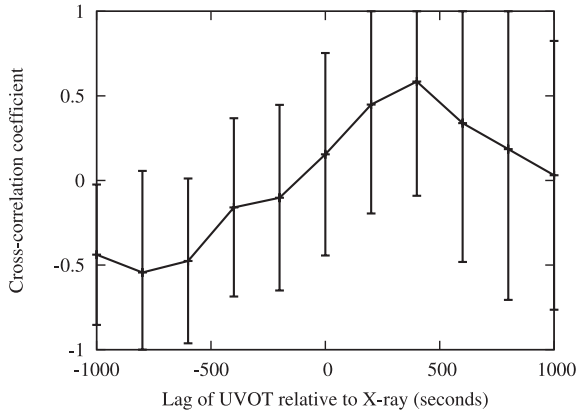
Figure 8. The very short time-scale (<1000 s) CCF between the X-ray and $uvw2$ bands calculated for the 2011 August ToO observations. The CCF shows a broad peak centred at a 400 s lag of the $uvw2$ behind the X-ray. The points are binned on 200 s time-scales as in the lightcurve in Fig. 3.

(2–10 keV) X-ray lightcurve from 2006, with exponential functions with various decay time-scales, and cross-correlated the resulting lightcurves with the observed *b*-band lightcurve. We find that the peak value of the CCF rises rapidly as the transfer function decay time-scale is increased from zero to $\sim$1 h. The largest peak CCF actually occurs with a decay time-scale of 1.7 orbits (2 h and 45 min), but the value of the peak does not change greatly between decay values of $\sim$1 h and a few hours.

4.3 Very short time-scales

In Fig. 8 we present the combined DCF (i.e. the weighted average of the DCFs for each segment) for the very short time-scale lightcurves shown in Fig. 3. These data hint at a lag of the $uvw2$ band by around 400 s, but are not sufficient for any definite conclusion to be drawn. They are, however, consistent with the DCF derived from the 2006 short-time-scale monitoring (Fig. 7) and with the *Chandra* and *HST* monitoring of O'Neill et al. (2006).

5   ACCRETION DISC MODELLING

As we have observations in four *UVOT* filters for each of the monitoring observations in 2008/2009 we are able to determine crude spectral energy distributions (SEDs) which we show in Fig. 9. Here we show both an SED from the average of all of the data and an SED representative of the highest flux levels. We can compare these SEDs with the prediction from a simple optically thick, geometrically thin, Shakura & Sunyaev (1973) accretion disc with constant accretion rate.

In our implementation we split the disc into 50 000 logarithmically spaced segments between $6R_\mathrm{g}$ and $60\,000R_\mathrm{g}$, covering almost all of the emission from the far-UV to far-IR. We assume a black hole mass of $3.6 \times 10^5\,\mathrm{M}_\odot$ (Peterson et al. 2005), an accretion rate of 0.1 per cent (Peterson et al. 2005), a distance of 4.2 Mpc (Thim et al. 2004) and place an X-ray point source at a height of $\sim 20R_\mathrm{g}$ above the central black hole. The albedo of the disc is assumed to be of the order of 0.3 (Gierliński, Done & Page 2009),and altering this value would just result in a scaling of the input L_x. We determine the integrated sum of the blackbody emission from each segment and fold it through the *UVOT* filter responses to determine the predicted count rates.
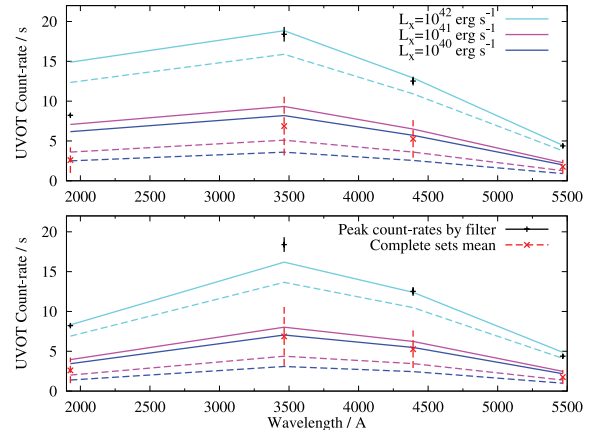
Figure 9. Spectral energy distributions. Top: the pure blackbody disc models plotted against the observed SEDs. Bottom: the reddened blackbody disc model plotted against the observed SEDs. The solid lines correspond to $\dot{m} = 10^{-3.0}\,\dot{m}_\mathrm{Edd}$ and the dashed lines to $\dot{m} = 10^{-3.5}\,\dot{m}_\mathrm{Edd}$. All count rates within each plot are scaled by the same factor.

We see that although the predicted and observed count rates can agree reasonably well at the red end of the spectrum (Fig. 9), the observed $uvw2$ count rate is a factor of 5 below the expected count rate. Although we have tried very hard to remove the background accurately, it is possible that a small systematic error exists which could account for any differences at the red end of the spectrum. However, it is not possible to account for the difference at the blue end by such errors. There are two simple explanations for this: the disc is truncated at a larger radius than $6R_\mathrm{g}$ or the observed spectrum is reddened by passage through some absorbing material. Given previous measurements of $A_V \sim 0.4$ mag (Lira et al. 1999) we prefer the reddening explanation. We require modest absorption of $E(B - V) \sim 0.14$ mag to reconcile the observed and predicted fluxes. For a standard Galactic dust to gas ratio this reddening corresponds to $N_\mathrm{H} \sim 1.0 \times 10^{21}\,\mathrm{cm}^{-2}$, which is quite consistent with the X-ray observations (Dwelly et al., in preparation). Also Lira et al. (1999) note that the Balmer decrement derived from the ratio of the fluxes of the narrow components of H_α and H_β is equivalent to an $A_V \sim 0.4$ mag, which is consistent with our observation with an $A_V \sim 0.44$ mag. The predicted count rates for a reddened face on disc are similar to the observed count rates, given the uncertainties in, e.g., distance or disc inclination angle.

6   DISCUSSION

We first list our main observational conclusions.

(i)   During monitoring from 2008 April to 2009 March with *Swift*, a large increase in flux was detected from NGC 4395 in the X-ray, UV and optical wavebands. This high flux period lasted for over 60 d, reaching X-ray flux levels at least five times greater than the previous average levels, before returning to those previous levels.

(ii)   There is a strong correlation between the UV/optical variations with peak CCF values of >0.9, and all show similar levels of fractional variability.

(iii)   The variations between the hard band X-rays (2–10 keV) and all *UVOT* bands are highly correlated with a lag consistent with zero days. The strength of these correlations decreases with increasing UV/optical wavelength.

(iv)   NGC 4395 was also observed once per *Swift* orbit, every orbit, for 5 d in 2006, using only the *b UVOT* filter. The lag was

again consistent with zero but the CCF was slightly asymmetric in the sense of a *b*-band lag of less than half a *Swift* orbit (i.e. <48 min).

(v) By splitting individual *Swift* ToO observations into 200 s bins, we find a weak correlation between the $uvw2$ and the X-ray lightcurves with a lag of ∼400 s.

(vi) The *UVOT* colours are consistent with the expectation from a standard optically thick accretion disc model, but only with the addition of a small amount of reddening.

These *Swift* observations, together with previous less extensive observations involving *Chandra* (Desroches et al. 2006), all indicate that the UV/optical emission in NGC 4395 probably lags behind the X-ray emission by a very short time-scale, certainly less than 48 min and more likely closer to a few hundred seconds. There are no observations which suggest that the UV/optical emission as observed on short (i.e. hours–day) time-scales leads the X-ray emission. An UV/optical lag of a few hundred seconds is consistent with the light-travel time to the UV/optical emission region in the accretion disc and thus strongly suggests that the short-time-scale UV/optical variations arise from reprocessing of X-ray emission.

If the UV/optical variability is driven mainly by reprocessing of X-ray emission, it is necessary that the variable component of the luminosity in the X-ray band exceeds that in the UV/optical bands. It is hard to measure the relative luminosities precisely as our observations do not cover all possible wavebands, but we can make an approximate calculation. For example, in Fig. 1 we see that the UV/optical variability is greatest in the $uvw2$ band where the range of fluxes is ∼4×10^{-15} ergs cm^{-2} s^{-1} Å^{-1}. In order to obtain the total variable UV/optical flux which might be driven by the X-rays we need to integrate over all UV/optical bands. If we take a total bandwidth of 1000 Å, and a flat spectrum, we would obtain a variable flux of ∼4×10^{-12} ergs cm^{-2} s^{-1}. For the Swift XRT a 2–10 keV flux of 1×10^{-11} ergs cm^{-2} s^{-1}, assuming a typical NGC 4395 photon index of 1.6, corresponds to ∼0.1 counts s^{-1}. Thus the variable 2–10 keV flux is ∼4×10^{-11} ergs cm^{-2} s^{-1}. Even allowing for the fact that probably less than half of the observed X-ray luminosity impinges upon the disc, this crude estimate indicates that there is probably sufficient luminosity in the X-ray variations to drive the UV/optical variability.

One might argue that simply extending the $uvw2$ variability over 1000 Å underestimates the total variable UV/optical luminosity. On the other hand, the 2–10 keV flux is less, by factors of a few, than the total irradiating X-ray flux, which may compensate. Other methods of estimating the total variable luminosity in the relevant bands, e.g. by modelling of the accretion disc, reach broadly the same conclusion. We therefore conclude that although there is probably not a great deal of room to spare, the luminosity in the X-ray band is just about sufficient to drive the UV/optical variability.

We also note that our treatment is rather simplistic. In reality the enhanced UV/optical emission which is produced by X-ray irradiation will probably lead to an enhanced flux of seed photons into the X-ray emitting corona, and hence to further X-ray emission. Thus variations in both bands may be prolonged in this feedback process. However, as long as the feedback is not too strong, the X-ray/UV-optical lag will remain as a valid indicator of the approximate separation of the emission regions.

The reason for the large outburst in 2008 is not entirely clear. Janiuk & Czerny (2011) suggest that disc radiation pressure instabilities, which might produce outbursts not too different from that seen, might occur in AGN such as NGC 4395 with a few-year time-scale. Janiuk & Czerny (2011) suggest that an accretion rate greater than 0.025 Eddington, which is probably just above that of

NGC 4395, is required for the instability to be relevant in AGN. However, given the uncertainties both in theoretical modelling and in estimating masses and accretion rates, this instability might still be relevant in NGC 4395. Alternatively the apparent outburst may just be part of the normal stochastic variability of the AGN. Although the X-ray flux in the 2011 monitoring observations did not reach the same level as in 2008, the mean 2011 flux level is a good deal higher than in the second part of the 2008–2009 monitoring observations and there are other similarities, e.g. softening of the spectrum with increasing flux (Dwelly et al., in preparation). We discuss the detailed temporal variability in more detail elsewhere (McHardy et al, in preparation) .

REFERENCES

Abazajian K. N. et al., 2009, ApJS, 182, 543
Arévalo P., Uttley P., Kaspi S., Breedt E., Lira P., McHardy I. M., 2008, MNRAS, 389, 1479
Arévalo P., Uttley P., Lira P., Breedt E., McHardy I. M., Churazov E., 2009, MNRAS, 397, 2004
Breedt E. et al., 2009, MNRAS, 394, 427
Breedt E. et al., 2010, MNRAS, 403, 605
Breeveld A. A. et al., 2010, MNRAS, 406, 1687
Burrows D. N. et al., 2005, Space Sci. Rev., 120, 165
Cackett E. M., Horne K., Winkler H., 2007, MNRAS, 380, 669
Collier S. J. et al., 1998, ApJ, 500, 162
Czerny B., 2006, in Gaskell C. M., McHardy I. M., Peterson B. M., Sergeev S. G., eds, ASP Conf. Ser. Vol. 360, AGN Variability from X-Rays to Radio Waves. Astron. Soc. Pac., San Francisco, p. 265
Desroches L.-B. et al., 2006, ApJ, 650, 88
Edelson R. A., Krolik J. H., 1988, ApJ, 333, 646
Fabian A. C. et al., 2012, MNRAS, 419, 116
Filippenko A. V., Ho L. C., 2003, ApJ, 588, L13
Filippenko A. V., Sargent W. L. W., 1989, ApJ, 342, L11
Gehrels N. et al., 2004, ApJ, 611, 1005
Gierliński M., Done C., Page K., 2009, MNRAS, 392, 1106
Janiuk A., Czerny B., 2011, MNRAS, 414, 2186
Kaaret P., Feng H., 2009, ApJ, 702, 1679
Krolik J. H., Horne K., Kallman T. R., Malkan M. A., Edelson R. A., Kriss G. A., 1991, ApJ, 371, 541
Lira P., Lawrence A., O'Brien P., Johnson R. A., Terlevich R., Bannister N., 1999, MNRAS, 305, 109
Lira P., Arévalo P., Uttley P., McHardy I., Breedt E., 2011, MNRAS, 415, 1290
Minezaki T. et al., 2006, ApJ, 643, L5
O'Neill P. M. et al., 2006, ApJ, 645, 160
Peng C. Y., Ho L. C., Impey C. D., Rix H.-W., 2002, AJ, 124, 266
Peng C. Y., Ho L. C., Impey C. D., Rix H.-W., 2010, AJ, 139, 2097
Peterson B. M. et al., 2005, ApJ, 632, 799
Peterson B. M. et al., 2006, ApJ, 641, 638
Poole T. S. et al., 2008, MNRAS, 383, 627
Roming P. W. A. et al., 2005, Space Sci. Rev., 120, 95
Roming P. W. A. et al., 2009, ApJ, 690, 163
Rowan-Robinson M. et al., 2008, MNRAS, 386, 697
Schlegel D. J., Finkbeiner D. P., Davis M., 1998, ApJ, 500, 525

Sergeev S. G., Doroshenko V. T., Golubinskiy Y. V., Merkulova N. I., Sergeeva E. A., 2005, ApJ, 622, 129

Shakura N. I., Sunyaev R. A., 1973, A&A, 24, 337

Thim F., Hoessel J. G., Saha A., Claver J., Dolphin A., Tammann G. A., 2004, AJ, 127, 2322

Timmer J., Koenig M., 1995, A&A, 300, 707

Uttley P., McHardy I. M., 2001, MNRAS, 323, L26

Vaughan S., Iwasawa K., Fabian A. C., Hayashida K., 2005, MNRAS, 356, 524

Wanders I. et al., 1997, ApJ, 113, 69

This paper has been typeset from a TEX/LATEX file prepared by the author.